Formulation and validation of the shift cell technique for acoustic applications of poro-elastic materials described by the Biot theory

Dario Magliacano[a,b,*], Sepide Ashani[c,e], Morvan Ouisse[a], Elke Deckers[d,e], Giuseppe Petrone[b], Wim Desmet[c,e], Sergio De Rosa[b]

[a] *FEMTO-ST Institute / Dep. of Applied Mechanics, Univ. Bourgogne Franche-Comté, CNRS/UFC/ENSMM/UTBM, Besançon, 25000, France*
[b] *Dep. of Industrial Engineering, Università di Napoli "Federico II", Corso Umberto I 40, Napoli, 80138, Italy*
[c] *KU Leuven, Department of Mechanical Engineering, Division LMSD, Celestijnenlaan 300, 2420 Heverlee, Belgium*
[d] *KU Leuven, Campus Diepenbeek, Department of Mechanical Engineering, Wetenschapspark 27, 3590 Diepenbeek, Belgium*
[e] *DMMS Lab, Flanders Make, 2420 Heverlee, Belgium*

Abstract

The inclusion of vibroacoustic treatments at early stage of product development through the use of poro-elastic media with periodic inclusions, which exhibit proper dynamic filtering effects, is a powerful strategy for the achievement of lightweight sound packages and represents a convenient solution for manufacturing aspects. This can have different applications in transportation (aerospace, automotive, railway), energy and civil engineering fields, where weight, space and vibroacoustic comfort are still critical challenges. This paper develops the shift cell operator approach as a numerical tool to investigate the dispersion characteristics of periodic poro-elastic media. It belongs to the class of the $k(\omega)$ (wave number as a function of the angular frequency) methods and leads to a quadratic eigenvalue problem, even when considering frequency-dependent materials, contrarily to the $\omega(k)$ approach that would lead to a non-linear eigenvalue problem for frequency-dependent materials.

*Corresponding author
Email address: dario.magliacano@univ-fcomte.fr, dario.magliacano@unina.it (Dario Magliacano)

The full formulation is detailed and the approach is successfully validate for a homogeneous poro-elastic material and a more complex periodic system containing periodic perfectly rigid circular inclusions.

Keywords: vibroacoustics, Biot theory of poro-elasticity, shift cell, FEM, dispersion diagram

---

1. Introduction

Fast urbanization and transport development cause serious noise-induced health risks, such as annoyance, sleep disturbance, or even ischemic heart disease [1]. Therefore, nowadays, environment noise control is becoming a subject of great interest. Generally, common sound absorbing materials could be divided into two categories: resonant [2] and poro-elastic materials. Resonant materials for sound absorption mainly involve Helmholtz resonators [3] and/or perforated panels [4]. These materials show good performances at low frequencies, but they often have the disadvantage of narrow frequency stop-bands [5]. Poro-elastic materials for acoustic applications are composed of channels, cracks or cavities that allow the sound waves entering the materials. Sound energy is dissipated by thermal and viscous losses; these energy consumption principles assure sound absorption over broader frequency ranges [6, 7]. Poro-elastic materials suffer from a lack of performance at low frequencies compared to their efficiency at higher ones [8]. This difficulty is usually overcome by multi-layering [9]; however, the efficiency of such devices relies on the allowable thickness [10, 11].

An efficient way to enhance the low frequency performances of sound packages consists in embedding periodic inclusions in a poro-elastic layer [12, 13], in order to create wave interferences or resonance effects that may be advantageous for the dynamics of the system. In this context of increasingly complex material systems, numerical tools to properly design sound packages are more and more useful. Several theoretical models are available to estimate the physical behavior of poro-elastic materials, and the most complex of them require the definition of more than ten parameters. For example, one of the most accurate models is the Biot theory of poro-elasticity [14], which takes into account both the mechanical and the acoustical behaviors of the material [15]. Furthermore, the measurement of all the necessary parameters, which usually constitutes the first step in the definition of a model, is already a specific issue in the case of poro-elastic.

In addition, numerical simulations, usually carried out through the Finite Element Method (FEM), are often problematic, in terms of computational times and convergence. On the other hand, analytical models constitute a powerful instrument to quickly catch physics and general trends of the problem, but they are partially limited by restrictive approximating hypotheses and come short considering non-trivial geometries. In this context, the present work investigates the application of the shift cell approach to poro-elastic media; this allows to obtain dispersion characteristics of frequency-dependent damped materials through the resolution of a quadratic eigenvalue problem, whose accuracy only depends on the FEM meshing. This technique has already been successfully applied to describe the mechanical behavior of periodic structures embedding visco-elastic materials [16, 17], piezoelectric materials [18] and foams modeled as equivalent fluids [19]. The main novelty of the present work consists in the formulation and application of the shift cell technique to Biot-modeled poro-elastic media. Materials modeled in this way account for wave propagation and interaction in both fluid and solid phases, thus leading to the fact that diphasic models are the most comprehensive ones in order to describe the vibroacoustics of porous media. However, compared to equivaled fluid models, they require more parameters to be used (a set for each of the two phases), and therefore the process of extension of the shift cell technique is definetly not trivial and requires a specific dissertation, which is herein provided for the first time in literature.

This paper is organized as it follows. Section 2 recalls the fundamentals of Biot theory and introduces the shift cell operator formulation for Biot-modeled foams. Section 2.2.2 defines a weak formulation of the problem, and Section Appendix B describes its FE implementation. In Section 3 two validations of the method are shown. At last, Section 4 provides conclusions and future perspectives.

2. Shift cell operator technique for Biot-modeled foams

2.1. Biot theory

Although for many porous materials the frame can be considered almost rigid for a wide range of acoustical frequencies, thus allowing the use of models with motionless skeleton assumption [20, 21], this is not generally true: for example, for a poro-elastic material attached to a vibrating structure and for many other similar situations, frame vibrations are induced by those of the elastic structure.

The wave propagation through a poro-elastic media can be analyzed only considering a solid-fluid coupled behavior; such description is provided by the Biot theory of sound propagation in poro-elastic media [14]. In this context, two compressional waves and a shear wave propagate. The parameters that characterize a poro-elastic material are: ϕ is the open porosity; σ is the static flow resistivity; α_∞ is the tortuosity; Λ is the viscous characteristic length; η_{visc} is the viscosity; $q_0 = \frac{\eta_{visc}}{\sigma}$ is the static viscous permeability; $\nu_{visc} = \frac{\eta_{visc}}{\rho_0}$; $\nu_{therm} = \frac{\nu_{visc}}{Pr}$; Pr is the Prandtl number. Furthermore, additional quantities are defined in Appendix A [22]. Zienkiewicz *et al.* proposed a simplified $\boldsymbol{u} - p$ formulation [23], where $\boldsymbol{u}$ is the solid phase displacement and p is the pressure of the fluid phase.

In particular, by neglecting the second time derivatives of the relative fluid displacement from the original Biot $\boldsymbol{u} - \boldsymbol{U}$ formulation [15], the $\boldsymbol{u} - p$ formulation [22, 24] is deduced in order to reduce the primary variables in the context of finite element analysis; indeed, if one considers a 3D model, instead of the 3+3 nodal variables that are in the $\boldsymbol{u} - \boldsymbol{U}$ formulation, in the case of the $\boldsymbol{u} - p$ one there are only 3+1 nodals variables. In addition, the solid displacement $\boldsymbol{u}$ and the pore fluid pressure p are always the most interesting quantities. In an infinite homogeneous isotropic poro-elastic media, three waves propagate (two compressional waves and one shear wave):

$$k_{shear} = \omega \sqrt{\frac{\tilde{\rho_{11}}\tilde{\rho_{22}} - \tilde{\rho_{12}}^2}{N\tilde{\rho_{22}}}}, \tag{1}$$

$$k_{fast,slow} = \sqrt{\frac{A_1}{2} \pm \sqrt{\frac{A_1^2}{4} - A_2}}, \text{with} \tag{2}$$

$$A_1 = \omega^2 \frac{\tilde{\rho_{11}}R - 2\tilde{\rho_{12}}Q + \tilde{\rho_{22}}P}{RP - Q^2},\ A_2 = \omega^4 \frac{\tilde{\rho_{11}}\tilde{\rho_{22}} - \tilde{\rho_{12}}^2}{RP - Q^2}. \tag{3}$$

The symbols introduced in Eq. 1-3 are defined in Appendix A. The two phases present in a poro-elastic material behave in a different manner, respect to the pure elastic case (where the onyl compressional wave is fluid-born): the main difference is the existence of a second (solid-born) compressional wave, which is highly attenuated in the low frequency range. Each of the waves propagates both in the solid and in the fluid phases of the poro-elastic medium [25].

2.2. Shift cell operator technique

2.2.1. Introduction

Herein, the shift cell operator technique applied to Biot-modeled foams is presented, providing details on its implementation [26]. The shift cell approach provides a reformulation of classical Floquet-Bloch periodic conditions [27], and its major advantage is that it allows the introduction of a generic frequency dependence of visco-elastic material behavior [16]; this is fundamental, if one looks for the computation of the dispersion curves of a porous material, modeled as an equivalent fluid or with the Biot theory. Indeed, even if the usage of Floquet-Bloch (F-B) periodic conditions actually allows it, a very powerful non-linear solver is required in that case.
The shift cell operator [16, 19], instead, leads to a quadratic eigenvalue problem even in the presence of frequency-dependences and/or damping. The main mathematical difference with respect to the classical F-B approach is that, in the case of the shift cell operator, the phase shift of the boundary conditions and the exponential amplitude decrease, related to wave propagation, are integrated into the partial derivative operator. As a consequence, the periodicity is included in the overall behavior of the structure, while simple continuity conditions are imposed at the edges of the unit cell.
Considering a poro-elastic layer modeled through Biot's theory [14], the coupled starting system is constituted by the equation of motion of the solid part and the classical Helmholtz equation, respectively:

$$\begin{cases} \boldsymbol{\nabla} \cdot \underline{\widehat{\sigma}}(\boldsymbol{u}) + \omega^2 \tilde{\rho} \boldsymbol{u} + \tilde{\gamma} \boldsymbol{\nabla} p = 0 \\ \\ \Delta p + \omega^2 \frac{\tilde{\rho_{22}}}{R} p - \omega^2 \frac{\tilde{\rho_{22}}}{\phi^2} \tilde{\gamma} \boldsymbol{\nabla} \cdot \boldsymbol{u} = 0 \end{cases}, \tag{4}$$

where $\boldsymbol{u} = (u, v, w)$ is the solid phase displacement vector and $p = p(\boldsymbol{x}, \omega)$ is the acoustic pressure [28]. The following quantities are defined [22]: ω is the angular frequency; $\underline{\widehat{\sigma}}(\boldsymbol{u}) = \underline{\underline{C}}\underline{\varepsilon}(\boldsymbol{u})$ is the stress tensor of the frame in vacuum, whose generic element can be written as $\sigma_{ij} = (\mu_1 - \frac{Q^2}{R})\delta_{ij}\varepsilon_{kk} + 2\mu_2\varepsilon_{ij}$, where δ_{ij} is the Kronecker delta and $\varepsilon_{kk} = tr(\underline{\varepsilon}) = \varepsilon_{ux} + \varepsilon_{vy} + \varepsilon_{wz}$; $\underline{\underline{C}}$ is the Hooke elasticity tensor with $C_{11} = \mu_1 - \frac{Q^2}{R} + 2\mu_2$ and $C_{12} = \mu_1 - \frac{Q^2}{R}$; $\underline{\varepsilon}(\boldsymbol{u}) = \frac{1}{2}(\boldsymbol{\nabla u} + \boldsymbol{\nabla u}^T)$ is the symmetric strain tensor; $\mu_1 = \frac{2\nu}{1-2\nu}N$ and $\mu_2 = N$ are respectively the first and second Lamé parameters.
For each physical property of the system, the periodicity is described by $\alpha(\boldsymbol{x} - r\boldsymbol{n}) - \alpha(\boldsymbol{x}) = 0$, where α is a generic physical property, $\boldsymbol{n}$ is a vector

of integers normal to the face considered, $\boldsymbol{r} = (r_1; r_2; r_3)$ is a matrix containing the three vectors defining the cell periodicity directions and lengths, and Ω is the domain of interest. This applies everywhere except on the discontinuity surfaces, where appropriate boundary conditions apply [19].
By further developing the latter equation and applying the Bloch theorem [29], which extends Floquet's theory to 3D systems, one obtains:

$$\begin{cases} (\boldsymbol{\nabla} + j\boldsymbol{k}) \cdot \underline{\underline{C}} \frac{1}{2}((\boldsymbol{\nabla} + j\boldsymbol{k})\boldsymbol{u} + (\boldsymbol{\nabla} + j\boldsymbol{k})\boldsymbol{u}^T) + \\ + \omega^2 \tilde{\rho}\boldsymbol{u} + \tilde{\gamma}(\boldsymbol{\nabla} + j\boldsymbol{k})p = \boldsymbol{0} \\ (\boldsymbol{\nabla} + j\boldsymbol{k})^T \cdot (\boldsymbol{\nabla} + j\boldsymbol{k})p + \omega^2 \frac{\tilde{\rho_{22}}}{R} p - \omega^2 \frac{\tilde{\rho_{22}}}{\phi^2} \tilde{\gamma}(\boldsymbol{\nabla} + j\boldsymbol{k}) \cdot \boldsymbol{u} = 0 \end{cases}, \tag{5}$$

with the wave vector $\boldsymbol{k}$ defined as:

$$\boldsymbol{k} = k\boldsymbol{\theta} = k \begin{pmatrix} \theta_x \\ \theta_y \\ \theta_z \end{pmatrix} = k \begin{pmatrix} \cos\theta \cos\phi \\ \cos\theta \sin\phi \\ \sin\theta \end{pmatrix} \tag{6}$$

and $k = -j\lambda$, where λ is an eigenvalue of the problem.

2.2.2. Weak formulation

The solution approach follows a common weak formulation of a differential problem in a discrete coordinate scheme. A $(\boldsymbol{u}, \boldsymbol{p})$ formulation, in its classical form, can be found in literature [24]:

$$\begin{cases} \int_\Omega \underline{\underline{\widehat{\sigma}}}(\boldsymbol{u}) : \underline{\underline{\varepsilon}}(\delta\boldsymbol{u}) \mathrm{d}\Omega - \omega^2 \int_\Omega \tilde{\rho}\boldsymbol{u} \cdot \delta\boldsymbol{u} \mathrm{d}\Omega + \\ - \int_\Omega (\tilde{\gamma} + \phi(1 + \frac{Q}{R}))\boldsymbol{\nabla} p \cdot \delta\boldsymbol{u} \mathrm{d}\Omega - \int_\Omega \phi(1 + \frac{Q}{R}) p\boldsymbol{\nabla} \cdot \delta\boldsymbol{u} \mathrm{d}\Omega + \\ - \int_\Gamma (\boldsymbol{\sigma_T}(\boldsymbol{u}, p) \cdot \boldsymbol{n}) \cdot \delta\boldsymbol{u} \mathrm{d}\Gamma = 0 \\ \int_\Omega \frac{\phi^2}{\omega^2 \tilde{\rho_{22}}} \boldsymbol{\nabla} p \cdot \boldsymbol{\nabla} \delta p \mathrm{d}\Omega - \int_\Omega \frac{\phi^2}{R} p\delta p \mathrm{d}\Omega + \\ - \int_\Omega (\gamma + \phi(1 + \frac{Q}{R}))\boldsymbol{\nabla}\delta p \cdot u \mathrm{d}\Omega - \int_\Omega \phi(1 + \frac{Q}{R})\delta p \boldsymbol{\nabla} \cdot u \mathrm{d}\Omega + \\ - \int_\Gamma \phi(U_n - u_n)\delta p \mathrm{d}\Gamma = 0 \end{cases}, \tag{7}$$

where $\delta\boldsymbol{u}$ and δp are admissible variations of the solid phase displacement vector and the interstitial fluid pressure of the poro-elastic medium, respectively. Considering that $\underline{\underline{\sigma}}(\boldsymbol{u}) = \underline{\underline{\underline{\underline{C}}}}\underline{\underline{\varepsilon}}(\boldsymbol{u}) = \underline{\underline{\underline{\underline{C}}}}\frac{1}{2}(\boldsymbol{\nabla u} + \boldsymbol{\nabla u}^T)$, and introducing the shift cell operator as explained above, one obtains:

145

$$\begin{cases} \int_\Omega (\underline{\underline{\underline{\underline{C}}}}\frac{1}{2}((\boldsymbol{\nabla} + j\boldsymbol{k})\boldsymbol{u} + (\boldsymbol{\nabla} + j\boldsymbol{k})\boldsymbol{u}^T)) : ((\boldsymbol{\nabla} - j\boldsymbol{k})\delta\boldsymbol{u} + (\boldsymbol{\nabla} - j\boldsymbol{k})\delta\boldsymbol{u}^T)\mathrm{d}\Omega + \\ -\omega^2 \int_\Omega \tilde{\rho}\boldsymbol{u}\cdot\delta\boldsymbol{u}\mathrm{d}\Omega - \int_\Omega (\tilde{\gamma} + \phi(1+\frac{Q}{R}))(\boldsymbol{\nabla} + j\boldsymbol{k})p\cdot\delta\boldsymbol{u}\mathrm{d}\Omega + \\ -\int_\Omega \phi(1+\frac{Q}{R})p(\boldsymbol{\nabla} - j\boldsymbol{k})\cdot\delta\boldsymbol{u}\mathrm{d}\Omega = 0 \\ \int_\Omega \frac{\phi^2}{\omega^2\tilde{\rho_{22}}}(\boldsymbol{\nabla} + j\boldsymbol{k})p\cdot(\boldsymbol{\nabla} - j\boldsymbol{k})\delta p\mathrm{d}\Omega + \\ -\int_\Omega \frac{\phi^2}{R}p\delta p\mathrm{d}\Omega - \int_\Omega (\tilde{\gamma} + \phi(1+\frac{Q}{R}))(\boldsymbol{\nabla} - j\boldsymbol{k})\delta p\cdot\boldsymbol{u}\mathrm{d}\Omega + \\ -\int_\Omega \phi(1+\frac{Q}{R})\delta p(\boldsymbol{\nabla} + j\boldsymbol{k})\cdot\boldsymbol{u}\mathrm{d}\Omega = 0 \end{cases}, \quad (8)$$

where the boundary condition caused the integral on the boundary to vanish. Therefore, one can define the following quantities:

- $\underline{\underline{\widehat{\sigma}_\theta}}(\boldsymbol{u}) = \underline{\underline{\underline{\underline{C}}}}\underline{\underline{\varepsilon_\theta}}(\boldsymbol{u})$, whose generic term is $\widehat{\sigma}_{\theta ij} = (\mu_1 - \frac{Q^2}{R})\delta_{ij}\varepsilon_{\theta kk} + 2\mu_2\varepsilon_{\theta ij}$;
- $\underline{\underline{\varepsilon_\theta}}(\boldsymbol{u}) = \frac{1}{2}(\boldsymbol{\theta u} + \boldsymbol{\theta u}^T)$.

Therefore:

$$\begin{cases} \int_\Omega \underline{\underline{\widehat{\sigma}}}(\boldsymbol{u}) : \underline{\underline{\varepsilon}}(\delta\boldsymbol{u})\mathrm{d}\Omega + jk \int_\Omega \underline{\underline{\widehat{\sigma_\theta}}}(\boldsymbol{u}) : \underline{\underline{\varepsilon}}(\delta\boldsymbol{u})\mathrm{d}\Omega + \\ - jk \int_\Omega \underline{\underline{\widehat{\sigma}}}(\boldsymbol{u}) : \varepsilon_{\underline{\underline{\boldsymbol{\theta}}}}(\delta\boldsymbol{u})\mathrm{d}\Omega + k^2 \int_\Omega \widehat{\sigma}_{\underline{\underline{\boldsymbol{\theta}}}}(\boldsymbol{u}) : \varepsilon_{\underline{\underline{\boldsymbol{\theta}}}}(\delta\boldsymbol{u})\mathrm{d}\Omega + \\ - \omega^2 \int_\Omega \tilde{\rho}\boldsymbol{u} \cdot \delta\boldsymbol{u}\mathrm{d}\Omega - \int_\Omega (\tilde{\gamma} + \phi(1 + \frac{Q}{R}))(\boldsymbol{\nabla} + j\boldsymbol{k})p \cdot \delta\boldsymbol{u}\mathrm{d}\Omega + \\ - \int_\Omega \phi(1 + \frac{Q}{R})p(\boldsymbol{\nabla} - j\boldsymbol{k}) \cdot \delta\boldsymbol{u}\mathrm{d}\Omega = 0 \\ \int_\Omega \frac{\phi^2}{\omega^2\tilde{\rho_{22}}} \boldsymbol{\nabla}p \cdot \boldsymbol{\nabla}\delta p\mathrm{d}\Omega + jk \int_\Omega \frac{\phi^2}{\omega^2\tilde{\rho_{22}}} \boldsymbol{\theta} \cdot p\boldsymbol{\nabla}\delta p\mathrm{d}\Omega + \\ - jk \int_\Omega \frac{\phi^2}{\omega^2\tilde{\rho_{22}}} \boldsymbol{\theta} \cdot \boldsymbol{\nabla}p\delta p\mathrm{d}\Omega + k^2 \int_\Omega \frac{\phi^2}{\omega^2\tilde{\rho_{22}}} p\delta p\mathrm{d}\Omega - \int_\Omega \frac{\phi^2}{R} p\delta p\mathrm{d}\Omega + \\ - \int_\Omega (\tilde{\gamma} + \phi(1 + \frac{Q}{R}))\boldsymbol{\nabla}\delta p \cdot \boldsymbol{u}\mathrm{d}\Omega + jk \int_\Omega (\tilde{\gamma} + \phi(1 + \frac{Q}{R}))\boldsymbol{\theta} \cdot \delta p\boldsymbol{u}\mathrm{d}\Omega + \\ - \int_\Omega \phi(1 + \frac{Q}{R})\delta p\boldsymbol{\nabla} \cdot \boldsymbol{u}\mathrm{d}\Omega - jk \int_\Omega \phi(1 + \frac{Q}{R})\boldsymbol{\theta} \cdot \delta p\boldsymbol{u}\mathrm{d}\Omega = 0 \end{cases}, \quad (9)$$

which can be written in a more structured form, as:

$$\begin{cases} \int_\Omega \underline{\underline{\widehat{\sigma}}}(\boldsymbol{u}) : \underline{\underline{\varepsilon}}(\delta\boldsymbol{u})\mathrm{d}\Omega + jk \int_\Omega (\widehat{\sigma}_{\underline{\underline{\boldsymbol{\theta}}}}(\boldsymbol{u}) : \underline{\underline{\varepsilon}}(\delta\boldsymbol{u}) - \underline{\underline{\widehat{\sigma}}}(\boldsymbol{u}) : \varepsilon_{\underline{\underline{\boldsymbol{\theta}}}}(\delta\boldsymbol{u}))\mathrm{d}\Omega + \\ + k^2 \int_\Omega \widehat{\sigma}_{\underline{\underline{\boldsymbol{\theta}}}}(\boldsymbol{u}) : \varepsilon_{\underline{\underline{\boldsymbol{\theta}}}}(\delta\boldsymbol{u})\mathrm{d}\Omega - \omega^2 \int_\Omega \tilde{\rho}\boldsymbol{u} \cdot \delta\boldsymbol{u}\mathrm{d}\Omega - \int_\Omega \tilde{\gamma}\boldsymbol{\nabla}p \cdot \delta\boldsymbol{u}\mathrm{d}\Omega + \\ - jk \int_\Omega \tilde{\gamma}\boldsymbol{\theta} \cdot p\delta\boldsymbol{u}\mathrm{d}\Omega - \int_\Omega \phi(1 + \frac{Q}{R})(\boldsymbol{\nabla}p \cdot \delta\boldsymbol{u} + p\boldsymbol{\nabla} \cdot \delta\boldsymbol{u})\mathrm{d}\Omega = 0 \\ \int_\Omega \frac{\phi^2}{\omega^2\tilde{\rho_{22}}} \boldsymbol{\nabla}p \cdot \boldsymbol{\nabla}\delta p\mathrm{d}\Omega + jk \int_\Omega \frac{\phi^2}{\omega^2\tilde{\rho_{22}}} (\boldsymbol{\theta} \cdot p\boldsymbol{\nabla}\delta p - \boldsymbol{\theta} \cdot \boldsymbol{\nabla}p\delta p)\mathrm{d}\Omega + \\ + k^2 \int_\Omega \frac{\phi^2}{\omega^2\tilde{\rho_{22}}} p\delta p\mathrm{d}\Omega - \int_\Omega \frac{\phi^2}{R} p\delta p\mathrm{d}\Omega - \int_\Omega \tilde{\gamma}\boldsymbol{\nabla}\delta p \cdot \boldsymbol{u}\mathrm{d}\Omega + \\ + jk \int_\Omega \tilde{\gamma}\boldsymbol{\theta} \cdot \delta p\boldsymbol{u}\mathrm{d}\Omega - \int_\Omega \phi(1 + \frac{Q}{R})(\boldsymbol{\nabla}\delta p \cdot \boldsymbol{u} + \delta p\boldsymbol{\nabla} \cdot \boldsymbol{u})\mathrm{d}\Omega = 0 \end{cases}. \quad (10)$$

Finally, one can discretize the weak formulation through the FE Method: considering that $\boldsymbol{\varphi_s}$ and $\boldsymbol{\varphi_f}$ are the eigenvectors of the solid and fluid parts respectively, the system of equations can be written in its matrix form:

$$\begin{cases} (\underline{\underline{K_s}} + jk\underline{\underline{L_s}} + k^2\underline{\underline{H_s}} - \omega^2\underline{\underline{M_s}})\boldsymbol{\varphi_s} - (\underline{\underline{N_s}} + jk\underline{\underline{O_s}} + \underline{\underline{T_s}})\boldsymbol{\varphi_f} = 0 \\ ((\underline{\underline{K_f}} + jk\underline{\underline{L_f}} + k^2\underline{\underline{H_f}} - \omega^2\underline{\underline{M_f}})\boldsymbol{\varphi_f} - \omega^2(\underline{\underline{N_f}} - jk\underline{\underline{O_f}} + \underline{\underline{T_f}})\boldsymbol{\varphi_s} = 0 \end{cases}, \quad (11)$$

with the following matrices ($\propto$ means "proportional to"):

- $\underline{\underline{K_s}} \propto \int_\Omega \underline{\underline{\widehat{\sigma}}}(\boldsymbol{u}) : \underline{\underline{\varepsilon}}(\delta\boldsymbol{u})\mathrm{d}\Omega$;
- $\underline{\underline{L_s}} \propto \int_\Omega (\underline{\underline{\widehat{\sigma}}}_{\underline{\underline{\boldsymbol{\theta}}}}(\boldsymbol{u}) : \underline{\underline{\varepsilon}}(\delta\boldsymbol{u}) - \underline{\underline{\widehat{\sigma}}}(\boldsymbol{u}) : \varepsilon_{\underline{\underline{\boldsymbol{\theta}}}}(\delta\boldsymbol{u}))\mathrm{d}\Omega$;
- $\underline{\underline{H_s}} \propto \int_\Omega \underline{\underline{\widehat{\sigma}}}_{\underline{\underline{\boldsymbol{\theta}}}}(\boldsymbol{u}) : \varepsilon_{\underline{\underline{\boldsymbol{\theta}}}}(\delta\boldsymbol{u})\mathrm{d}\Omega$;
- $\underline{\underline{M_s}} \propto \int_\Omega \tilde{\rho}\boldsymbol{u} \cdot \delta\boldsymbol{u}\mathrm{d}\Omega$;
- $\underline{\underline{N_s}} \propto \int_\Omega \tilde{\gamma}\boldsymbol{\nabla} p \cdot \delta\boldsymbol{u}\mathrm{d}\Omega$;
- $\underline{\underline{O_s}} \propto \int_\Omega \tilde{\gamma}\boldsymbol{\theta} \cdot p\delta\boldsymbol{u}\mathrm{d}\Omega$;
- $\underline{\underline{T_s}} \propto \int_\Omega \phi(1 + \frac{Q}{R})(\boldsymbol{\nabla} p \cdot \delta\boldsymbol{u} + p\boldsymbol{\nabla} \cdot \delta\boldsymbol{u})\mathrm{d}\Omega$;
- $\underline{\underline{K_f}} \propto \int_\Omega \frac{\phi^2}{\tilde{\rho_{22}}}\boldsymbol{\nabla} p \cdot \boldsymbol{\nabla}\delta p\mathrm{d}\Omega$;
- $\underline{\underline{L_f}} \propto \int_\Omega \frac{\phi^2}{\tilde{\rho_{22}}}(\boldsymbol{\theta} \cdot p\boldsymbol{\nabla}\delta p - \boldsymbol{\theta} \cdot \boldsymbol{\nabla} p\delta p)\mathrm{d}\Omega$;
- $\underline{\underline{H_f}} \propto \int_\Omega \frac{\phi^2}{\tilde{\rho_{22}}} p\delta p\mathrm{d}\Omega$;
- $\underline{\underline{M_f}} \propto \int_\Omega \frac{\phi^2}{R} p\delta p\mathrm{d}\Omega$;
- $\underline{\underline{N_f}} \propto \int_\Omega \tilde{\gamma}\boldsymbol{\nabla}\delta p \cdot \boldsymbol{u}\mathrm{d}\Omega$;
- $\underline{\underline{O_f}} \propto \int_\Omega \tilde{\gamma}\boldsymbol{\theta} \cdot \delta p\boldsymbol{u}\mathrm{d}\Omega$;
- $\underline{\underline{T_f}} \propto \int_\Omega \phi(1 + \frac{Q}{R})(\boldsymbol{\nabla}\delta p \cdot \boldsymbol{u} + \delta p\boldsymbol{\nabla} \cdot \boldsymbol{u})\mathrm{d}\Omega$.

Here, $\underline{\underline{M_{s,f}}}$ and $\underline{\underline{K_{s,f}}}$ are respectively the symmetric mass and symmetric stiffness matrices, $\underline{\underline{L_{s,f}}}$ are skew-symmetric matrices, $\underline{\underline{H_{s,f}}}$ are symmetric matrices and $\underline{\underline{N_s}} = \underline{\underline{N_f}}^T$, $\underline{\underline{O_s}} = \underline{\underline{O_f}}^T$ and $\underline{\underline{T_s}} = \underline{\underline{T_f}}^T$ are the matrices that couple the solid and fluid behaviors; all of them are complex and frequency-dependent. Therefore, the coupled system can be written as it follows:

$$\begin{bmatrix} (\underline{\underline{K_s}} + jk\underline{\underline{L_s}} + k^2\underline{\underline{H_s}} - \omega^2\underline{\underline{M_s}}) & -(\underline{\underline{N_f}} - jk\underline{\underline{O_f}} + \underline{\underline{T_f}}) \\ -(\underline{\underline{N_s}} + jk\underline{\underline{O_s}} + \underline{\underline{T_s}}) & \frac{1}{\omega^2}(\underline{\underline{K_f}} + jk\underline{\underline{L_f}} + k^2\underline{\underline{H_f}} - \omega^2\underline{\underline{M_f}}) \end{bmatrix} \begin{pmatrix} \boldsymbol{\varphi_s} \\ \boldsymbol{\varphi_f} \end{pmatrix} = \\ = \begin{pmatrix} 0 \\ 0 \end{pmatrix}. \tag{12}$$

The details of the FE implementation are given in Appendix B.

3. Validation of the method

In order to validate the shift cell technique implementation for Biot-modeled foams and for waves propagating along the x-axis, two different comparisons are provided: one with an application of the shift cell approach to an equivalent fluid [19], and another one with a WFEM analysis performed on a Biot-modeled foam [25].

3.1. Biot model with shift cell vs. JCA model with shift cell

The first considered system is a homogeneous foam with material properties shown in Table 1, represented by a cubic unit cell having a volume of 8 cm^3, with periodicity in three directions and mesh composed by 10 thetraedral elements along each side of the cube. The second case is constructed by introducing a rigid cylindrical inclusion with radius equal to 0.5 cm at the center of the previous unit cell, as shown in Figure 1.

In Figure 2 and Figure 3, dispersion curves of two different systems with an artificially high value of frame Young modulus ($E = 10^{15}$ Pa) and nullified loss factor, such that the rigid frame assumption would be valid, are calculated using the shift cell approach and compare the results obtained through the Biot model with those calculated using a Johnson-Champoux-Allard (JCA) [30, 31] equivalent fluid [19]. Therefore, the elasticity of the skeleton is neglected and the Biot model essentially describes the behavior of the equivalent fluid one. The distinction between propagative and evanescent waves is obtained, in a first approximation, through the application of the 1^{st} classifying criterion described by Magliacano *et al.* [19] for equivalent fluids. Looking at Figure 2 and Figure 3, it can be noticed that the comparison shows an almost perfect agreement between the results of the shift cell technique applied on the two different foam models. The advantage of using Biot model, for which the shift cell approach is developed herein, relies on the fact that, as already introduced in Section 1, in some cases (for example: low-frequency acoustic loads, or mechanical excitations) waves can propagate in both fluid and solid phases. In those contexts, motionless skeleton models cannot be used and a more general diphasic model (like Biot's one) is required in order to describe the poro-elastic behavior of the foam [32]. Moreover, if the frequency range of the study is under the decoupling frequency, which is located at high frequencies for foams with high value of flow resistivity, the

Porosity	0.98	**Density** [kg/m^3]	22.1
Tortuosity	1.17	**Young modulus** [kPa]	70+j9
Resistivity [Pa*s/m^2]	3750	**Shear modulus** [kPa]	25+j7
Viscous char. length [mm]	0.11	**Loss factor**	0.265
Thermal char. length [mm]	0.742	**Poisson ratio**	0.39

Table 1: Properties of a PU 60 foam.

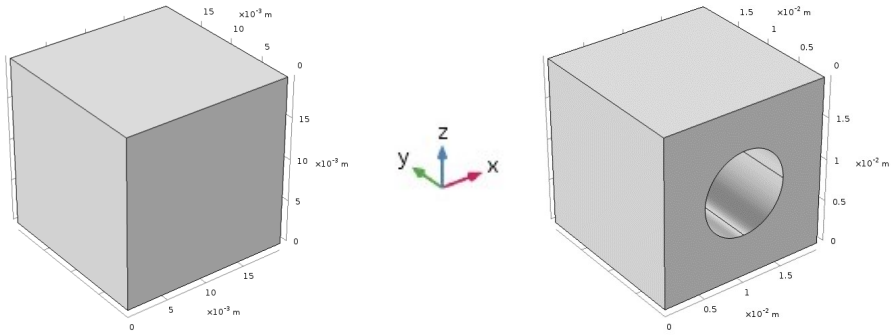

Figure 1: 3D unit cell constituted by a 2 cm cube, homogeneous (on the left) and with a 5 mm radius cylindrical hole (on the right).

equivalent fluid model prediction deviates significantly from the Biot theory; therefore, also in these cases it is necessary to use the latter, in order to have an accurate overview of the wave propagation in the medium. In addition, as it is more clear in Figure 4 and Figure 5, the shift cell approach is capable to catch the behavior of the three types of waves propagating in a porous material with elastic frame.

3.2. Biot model with shift cell vs. Biot model with WFEM

In this validation case, shift cell results are compared to those obtained by Serra *et al.* [25] using the Wave Finite Element Method [33] (labeled as "reference" in Figure 4 and Figure 5). Parameters of foam and air used in this validation case can be found in Appendix B of Serra *et al.* [25], and are reported here in Table 2 and Table 3. In the case of poro-elastic media the rigidity of the material is very low, leading to very small wavelengths, and a high dissipation rate occurs within the pores; despite these difficulties, in the paper by Serra *et al.* [25] it is shown that the WFEM provides an efficient tool to compute the waves propagating through poro-elastic media.

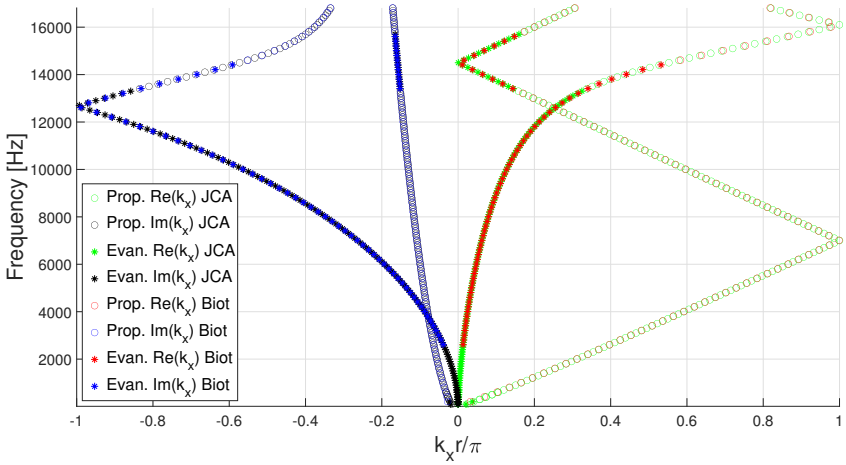

Figure 2: Dispersion curves validation with JCA plots; here, the Biot curves are computed for a homogeneous PU 60 foam, with $E = 10^{15}$ Pa and structural loss factor $= 0$.

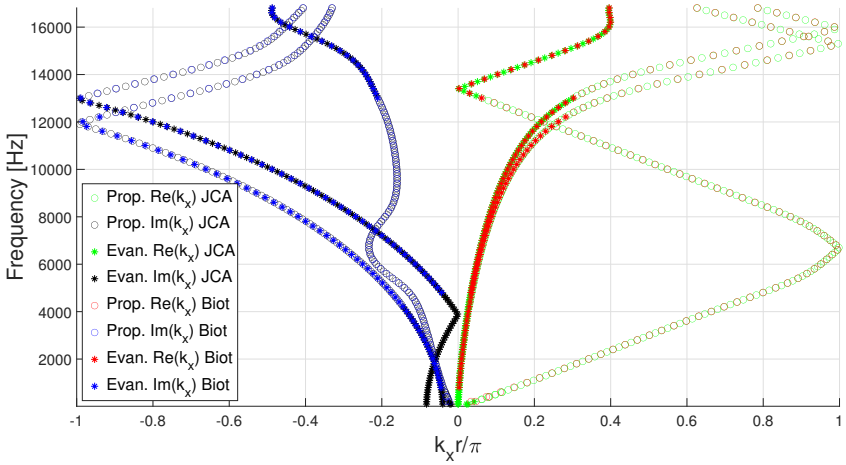

Figure 3: Dispersion curves validation with JCA plots; here, the Biot curves are computed for a PU 60 foam with a perfectly rigid cylindrical inclusion, with $E = 10^{15}$ Pa and structural loss factor $= 0$.

Porosity	0.96	**Density** [kg/m^3]	30
Tortuosity	1.7	**Young modulus** [kPa]	733+j73
Resistivity [Pa*s/m^2]	32000	**Shear modulus** [kPa]	264+j26
Viscous char. length [mm]	0.09	**Loss factor**	0.1
Thermal char. length [mm]	0.165	**Poisson ratio**	0.387

Table 2: Properties of the foam used in the validation with the work by Serra *et al.* [25].

Ambient fluid density [kg/m^3]	1.21
Ambient fluid dynamic viscosity [N/(m*s)]	1.84*10^{-5}
Standard pressure [Pa]	101325
Heat capacity ratio	1.4
Prandtl's number	0.71

Table 3: Properties of the air used in the validation with the work by Serra *et al.* [25].

This validation is also performed with curves computed through the analytical model described in Section 2.1. As it is clear in Figure 4 and Figure 5, wavenumbers calculated using the shift cell approach applied to a Biot-modeled foam completely agree with those calculated through the analytical model; moreover, it can be seen that the slow compressional wave is highly attenuated.

The shift cell approach has several advantages, in terms of linearity and convergence, compared to the WFEM. Indeed, as described by Serra *et al.* [25], the WFEM applied to Biot-modeled foams leads to a transcendental eigenvalue problem that can be solved only by using a nonlinear solver. However, there are still a lot of numerical difficulties, and robust solutions have not yet been developed [34].

In the case of WFEM, the use of 10 elements per wavelength in the three directions is recommended as a rule of the thumb [25]. Under the hypotheses of plane wave, the use of the shift cell approach leads directly to a quadratic eigenvalue problem, with no assumption on the nature of the waves, whose accuracy only depends on the mesh chosen to discretize the system.

4. Conclusions

An efficient way to enhance the low frequency performances of sound packages consists in embedding periodic inclusions in a poro-elastic layer, in

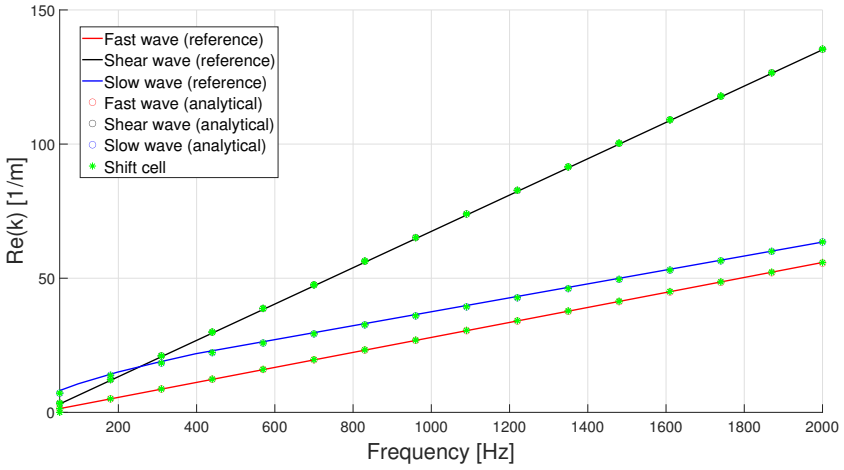

Figure 4: Dispersion curve comparison with the reference (WFEM by Serra *et al.* [25]), and analytical model; real part of the wavenumber.

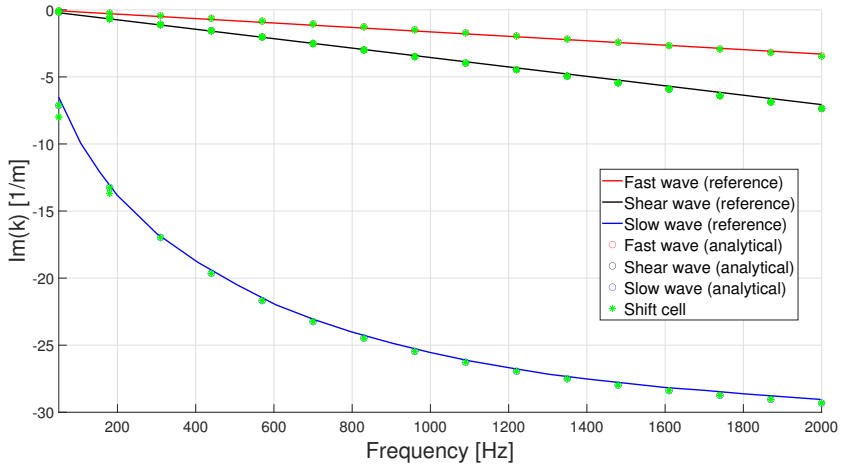

Figure 5: Dispersion curve comparison with the reference (WFEM by Serra *et al.* [25]), and analytical model; imaginary part of the wavenumber.

order to create wave interferences or resonance effects that may be advantageous for the dynamics of the system. This work develops the shift cell technique as a numerical tool to investigate the dispersion characteristics of periodic Biot-modeled poro-elastic media, providing details on its FEM implementation too; this approach allows to obtain dispersion characteristics of frequency-dependent damped materials through the resolution of a quadratic eigenvalue problem, whose accuracy only depends on the FEM meshing. A first validation of the shift cell approach for Biot-modeled poro-elastic materials has been obtained through a comparison with the results obtained on a JCA-modeled 3D unit cell, both in a homogeneous configuration and with a perfectly rigid cylindrical inclusion. For this purpose, the elasticity of the foam skeleton has been neglected and therefore the Biot model essentially described the behavior of an equivalent fluid, thus allowing the comparison between dispersion curves obtained through the application of the shift cell approach to Biot-modeled foams and equivalent fluids.
An additional validation has then been carried out through a comparison of the shift cell results with those obtained using the Wave Finite Element Method, and those computed through an analytical model that is valid for infinite homogeneous isotropic poro-elastic media; in this context, compared to the WFEM, the shift cell technique shows significant computational advantages. The outcome of this research is very promising, since the methodological basis and its validations are given in order to trace future characterizations and applications of periodic poro-elastic media in acoustics.

Appendix A. Quantities defined in Biot model of poro-elasticity

- $A_1 = \omega^2 \frac{\tilde{\rho_{11}} R - 2\tilde{\rho_{12}} Q + \tilde{\rho_{22}} P}{RP - Q^2}$;
- $A_2 = \omega^4 \frac{\tilde{\rho_{11}}\tilde{\rho_{22}} - \tilde{\rho_{12}}^2}{RP - Q^2}$;
- $\tilde{\rho_{11}}$, $\tilde{\rho_{12}}$ and $\tilde{\rho_{22}}$ are parameters depending on the nature and the geometry of the poro-elastic medium and the density of the fluid; in particular: $\tilde{\rho_{11}} = \rho_1 + \rho_a + \frac{b}{j\omega}$, $\tilde{\rho_{12}} = -\rho_a - \frac{b}{j\omega}$, $\tilde{\rho_{22}} = \phi\rho_0 + \rho_a + \frac{b}{j\omega}$;
- ρ_0 is the bulk density of the fluid phase;
- ρ_1 is the bulk density of the solid phase;
- $\rho_a = \phi\rho_0(\alpha_\infty - 1)$ is an inertial coupling term;

- $b = \sigma\phi^2 G(\omega)$ is the viscous drag;
- $G(\omega) = \sqrt{1 + \frac{4j\alpha_\infty^2 \eta_{visc}\rho_0\omega}{(\sigma\Lambda\phi)^2}}$ is the relaxation function, as predicted by JCA model [30, 31];
- $\tilde{\rho} = (\tilde{\rho_{11}} - \frac{\tilde{\rho_{12}}^2}{\tilde{\rho_{22}}})$;
- P, Q, R are elasticity coefficients to be determined by "gedanken experiments" [21]; in particular [20]: $P = \frac{(1-\phi)(1-\phi-\frac{KB}{KS})KS+\phi\frac{KBKS}{KF}}{1-\phi-\frac{KB}{KS}+\phi\frac{KS}{KF}} - \frac{2}{3}N \cong (1 + \frac{\nu}{1-2\nu})2N + \frac{1-\phi^2}{\phi}KF$, $Q = \frac{(1-\phi-\frac{KB}{KS})\phi KS}{1-\phi-\frac{KB}{KS}+\phi\frac{KS}{KF}} \cong (1-\phi)KF$, $R = \frac{\phi^2 KS}{1-\phi-\frac{KB}{KS}+\phi\frac{KS}{KF}} \cong \phi KF$;
- $N = |N|(1 + j\eta) = \frac{Y}{2(1+\nu)}$ is the complex shear modulus of the frame;
- $Y = |Y|(1 + j\eta)$ is the complex Young modulus of the frame;
- η is the loss factor of the frame;
- ν is the Poisson's ratio of the frame;
- $KB = \frac{2N(\nu+1)}{3(1-2\nu)}$ is the bulk modulus of the the solid phase in vacuum;
- $KS = \frac{KB}{1-\phi}$ is the bulk modulus of the solid phase;
- KF is the bulk modulus of the fluid phase, computed starting from the equivalent one (e.g.: $KF = \phi K_{JCA}$);
- $\tilde{\gamma} = \phi(\frac{\tilde{\rho_{12}}}{\tilde{\rho_{22}}} - \frac{Q}{R})$;
- $\mu_i = \frac{P\delta_i^2 - \omega^2\tilde{\rho_{11}}}{\omega^2\tilde{\rho_{12}} - Q\delta_i^2}, i = 1, 2$ is the ratio of the velocity of the air over the velocity of the frame for the two compressional waves and indicates in what medium the waves propagate preferentially.

Appendix B. Finite element implementation

In order to numerically implement the shift cell technique for Biot-modeled foams, the vector equation related to the motion of the solid part is split into

three scalar equations. The following matrices are defined accordingly:

$$\boldsymbol{u} = \begin{pmatrix} u \\ v \\ w \end{pmatrix}, \boldsymbol{\nabla u} = \begin{bmatrix} \frac{\partial u}{\partial x} & \frac{\partial v}{\partial x} & \frac{\partial w}{\partial x} \\ \frac{\partial u}{\partial y} & \frac{\partial v}{\partial y} & \frac{\partial w}{\partial y} \\ \frac{\partial u}{\partial z} & \frac{\partial v}{\partial z} & \frac{\partial w}{\partial z} \end{bmatrix}, \boldsymbol{\theta u} = \begin{bmatrix} \theta_x u & \theta_x v & \theta_x w \\ \theta_y u & \theta_y v & \theta_y w \\ \theta_z u & \theta_z v & \theta_z w \end{bmatrix}, \tag{B.1}$$

$$\underline{\underline{\varepsilon}}(\boldsymbol{u}) = \begin{bmatrix} \frac{\partial u}{\partial x} & \frac{1}{2}(\frac{\partial u}{\partial y} + \frac{\partial v}{\partial x}) & \frac{1}{2}(\frac{\partial u}{\partial z} + \frac{\partial w}{\partial x}) \\ \frac{1}{2}(\frac{\partial u}{\partial y} + \frac{\partial v}{\partial x}) & \frac{\partial v}{\partial y} & \frac{1}{2}(\frac{\partial v}{\partial z} + \frac{\partial w}{\partial y}) \\ \frac{1}{2}(\frac{\partial u}{\partial z} + \frac{\partial w}{\partial x}) & \frac{1}{2}(\frac{\partial v}{\partial z} + \frac{\partial w}{\partial y}) & \frac{\partial w}{\partial z} \end{bmatrix}, \tag{B.2}$$

$$\underline{\underline{\varepsilon_\theta}}(\boldsymbol{u}) = \begin{bmatrix} \theta_x u & \frac{1}{2}(\theta_y u + \theta_x v) & \frac{1}{2}(\theta_z u + \theta_x w) \\ \frac{1}{2}(\theta_y u + \theta_x v) & \theta_y v & \frac{1}{2}(\theta_z v + \theta_y w) \\ \frac{1}{2}(\theta_z u + \theta_x w) & \frac{1}{2}(\theta_z v + \theta_y w) & \theta_z w \end{bmatrix}, \tag{B.3}$$

$$\underline{\underline{\widehat{\sigma}}}(\boldsymbol{u}) = \begin{bmatrix} C_{11}\frac{\partial u}{\partial x} + C_{12}(\frac{\partial v}{\partial y} + \frac{\partial w}{\partial z}) & (C_{11} - C_{12})\frac{1}{2}(\frac{\partial u}{\partial y} + \frac{\partial v}{\partial x}) & (C_{11} - C_{12})\frac{1}{2}(\frac{\partial u}{\partial z} + \frac{\partial w}{\partial x}) \\ (C_{11} - C_{12})\frac{1}{2}(\frac{\partial u}{\partial y} + \frac{\partial v}{\partial x}) & C_{11}\frac{\partial v}{\partial y} + C_{12}(\frac{\partial u}{\partial x} + \frac{\partial w}{\partial z}) & (C_{11} - C_{12})\frac{1}{2}(\frac{\partial v}{\partial z} + \frac{\partial w}{\partial y}) \\ (C_{11} - C_{12})\frac{1}{2}(\frac{\partial u}{\partial z} + \frac{\partial w}{\partial x}) & (C_{11} - C_{12})\frac{1}{2}(\frac{\partial v}{\partial z} + \frac{\partial w}{\partial y}) & C_{11}\frac{\partial w}{\partial z} + C_{12}(\frac{\partial u}{\partial x} + \frac{\partial v}{\partial y}) \end{bmatrix} \tag{B.4}$$

$$\underline{\underline{\widehat{\sigma}_\theta}}(\boldsymbol{u}) = \begin{bmatrix} C_{11}\theta_x u + C_{12}(\theta_y v + \theta_z w) & (C_{11} - C_{12})\frac{1}{2}(\theta_y u + \theta_x v) & (C_{11} - C_{12})\frac{1}{2}(\theta_z u + \theta_x w) \\ (C_{11} - C_{12})\frac{1}{2}(\theta_y u + \theta_x v) & C_{11}\theta_y v + C_{12}(\theta_x u + \theta_z w) & (C_{11} - C_{12})\frac{1}{2}(\theta_z v + \theta_y w) \\ (C_{11} - C_{12})\frac{1}{2}(\theta_z u + \theta_x w) & (C_{11} - C_{12})\frac{1}{2}(\theta_z v + \theta_y w) & C_{11}\theta_z w + C_{12}(\theta_x u + \theta_y v) \end{bmatrix} \tag{B.5}$$

The numerical model is based on the following matrix weak formulation, proposed to provide an expression optimized for the FE implementation:

- $\underline{\underline{K_{s,u}}} \propto \int_\Omega ((C_{11}\frac{\partial u}{\partial x} + C_{12}(\frac{\partial v}{\partial y} + \frac{\partial w}{\partial z}))\frac{\partial \delta u}{\partial x} + (C_{11} - C_{12})\frac{1}{4}((\frac{\partial u}{\partial y} + \frac{\partial v}{\partial x})(\frac{\partial \delta u}{\partial y} + \frac{\partial \delta v}{\partial x}) + (\frac{\partial u}{\partial z} + \frac{\partial w}{\partial x})(\frac{\partial \delta u}{\partial z} + \frac{\partial \delta w}{\partial x})))\mathrm{d}\Omega$;
- $\underline{\underline{L_{s,u}}} \propto \int_\Omega ((C_{11}\theta_x u + C_{12}(\theta_y v + \theta_z w))\frac{\partial \delta u}{\partial x} + (C_{11} - C_{12})\frac{1}{4}((\theta_y u + \theta_x v)(\frac{\partial \delta u}{\partial y} + \frac{\partial \delta v}{\partial x}) + (\theta_z u + \theta_x w)(\frac{\partial \delta u}{\partial z} + \frac{\partial \delta w}{\partial x})) - (C_{11}\frac{\partial u}{\partial x} + C_{12}(\frac{\partial v}{\partial y} + \frac{\partial w}{\partial z}))\theta_x \delta u - (C_{11} - C_{12})\frac{1}{4}((\frac{\partial u}{\partial y} + \frac{\partial v}{\partial x})(\theta_y \delta u + \theta_x \delta v) + (\frac{\partial u}{\partial z} + \frac{\partial w}{\partial x})(\theta_z \delta u + \theta_x \delta w)))\mathrm{d}\Omega$;
- $\underline{\underline{H_{s,u}}} \propto \int_\Omega ((C_{11}\theta_x u + C_{12}(\theta_y v + \theta_z w))\theta_x \delta u + (C_{11} - C_{12})\frac{1}{4}((\theta_y u + \theta_x v)(\theta_y \delta u + \theta_x \delta v) + (\theta_z u + \theta_x w)(\theta_z \delta u + \theta_x \delta w)))\mathrm{d}\Omega$;
- $\underline{\underline{M_{s,u}}} \propto \int_\Omega \tilde{\rho} u \delta u \mathrm{d}\Omega$;

- $\underline{\underline{N_{s,u}}} \propto \int_\Omega \tilde{\gamma}\frac{\partial p}{\partial x}\delta u \mathrm{d}\Omega$;
- $\underline{\underline{O_{s,u}}} \propto \int_\Omega \tilde{\gamma}\theta_1 p\delta u \mathrm{d}\Omega$;
- $\underline{\underline{T_{s,u}}} \propto \int_\Omega \phi(1+\frac{Q}{R})(\frac{\partial p}{\partial x}\delta u + p\frac{\partial \delta u}{\partial x})\mathrm{d}\Omega$;
- $\underline{\underline{K_{s,v}}} \propto \int_\Omega((C_{11}\frac{\partial v}{\partial y}+C_{12}(\frac{\partial u}{\partial x}+\frac{\partial w}{\partial z}))\frac{\partial \delta v}{\partial y}+(C_{11}-C_{12})\frac{1}{4}((\frac{\partial u}{\partial y}+\frac{\partial v}{\partial x})(\frac{\partial \delta u}{\partial y}+\frac{\partial \delta v}{\partial x})+(\frac{\partial v}{\partial z}+\frac{\partial w}{\partial y})(\frac{\partial \delta v}{\partial z}+\frac{\partial \delta w}{\partial y})))\mathrm{d}\Omega$;
- $\underline{\underline{L_{s,v}}} \propto \int_\Omega((C_{11}\theta_y v+C_{12}(\theta_x u+\theta_z w))\frac{\partial \delta v}{\partial y}+(C_{11}-C_{12})\frac{1}{4}((\theta_y u+\theta_x v)(\frac{\partial \delta u}{\partial y}+\frac{\partial \delta v}{\partial x})+(\theta_z v+\theta_y w)(\frac{\partial \delta v}{\partial z}+\frac{\partial \delta w}{\partial y}))-(C_{11}\frac{\partial v}{\partial y}+C_{12}(\frac{\partial u}{\partial x}+\frac{\partial w}{\partial z}))\theta_y\delta v-(C_{11}-C_{12})\frac{1}{4}((\frac{\partial u}{\partial y}+\frac{\partial v}{\partial x})(\theta_y\delta u+\theta_x\delta v)+(\frac{\partial v}{\partial z}+\frac{\partial w}{\partial y})(\theta_z\delta v+\theta_y\delta w)))\mathrm{d}\Omega$;
- $\underline{\underline{H_{s,v}}} \propto \int_\Omega((C_{11}\theta_y v+C_{12}(\theta_x u+\theta_z w))\theta_y\delta v+(C_{11}-C_{12})\frac{1}{4}((\theta_y u+\theta_x v)(\theta_y\delta u+\theta_x\delta v)+(\theta_z v+\theta_y w)(\theta_z\delta v+\theta_y\delta w)))\mathrm{d}\Omega$;
- $\underline{\underline{M_{s,v}}} \propto \int_\Omega \tilde{\rho} v\delta v \mathrm{d}\Omega$;
- $\underline{\underline{N_{s,v}}} \propto \int_\Omega \tilde{\gamma}\frac{\partial p}{\partial y}\delta v \mathrm{d}\Omega$;
- $\underline{\underline{O_{s,v}}} \propto \int_\Omega \tilde{\gamma}\theta_2 p\delta v \mathrm{d}\Omega$;
- $\underline{\underline{T_{s,v}}} \propto \int_\Omega \phi(1+\frac{Q}{R})(\frac{\partial p}{\partial y}\delta v + p\frac{\partial \delta v}{\partial y})\mathrm{d}\Omega$;
- $\underline{\underline{K_{s,w}}} \propto \int_\Omega((C_{11}\frac{\partial w}{\partial z}+C_{12}(\frac{\partial u}{\partial x}+\frac{\partial v}{\partial y}))\frac{\partial \delta w}{\partial z}+(C_{11}-C_{12})\frac{1}{4}((\frac{\partial v}{\partial z}+\frac{\partial w}{\partial y})(\frac{\partial \delta v}{\partial z}+\frac{\partial \delta w}{\partial y})+(\frac{\partial u}{\partial z}+\frac{\partial w}{\partial x})(\frac{\partial \delta u}{\partial z}+\frac{\partial \delta w}{\partial x})))\mathrm{d}\Omega$;
- $\underline{\underline{L_{s,w}}} \propto \int_\Omega((C_{11}\theta_z w+C_{12}(\theta_x u+\theta_y v))\frac{\partial \delta w}{\partial z}+(C_{11}-C_{12})\frac{1}{4}((\theta_y w+\theta_z v)(\frac{\partial \delta w}{\partial y}+\frac{\partial \delta v}{\partial z})+(\theta_z u+\theta_x w)(\frac{\partial \delta u}{\partial z}+\frac{\partial \delta w}{\partial x}))-(C_{11}\frac{\partial w}{\partial z}+C_{12}(\frac{\partial u}{\partial x}+\frac{\partial v}{\partial y}))\theta_z\delta w-(C_{11}-C_{12})\frac{1}{4}((\frac{\partial w}{\partial y}+\frac{\partial v}{\partial z})(\theta_y\delta w+\theta_z\delta v)+(\frac{\partial u}{\partial z}+\frac{\partial w}{\partial x})(\theta_z\delta u+\theta_x\delta w)))\mathrm{d}\Omega$;
- $\underline{\underline{H_{s,w}}} \propto \int_\Omega((C_{11}\theta_z w+C_{12}(\theta_x u+\theta_y v))\theta_z\delta w+(C_{11}-C_{12})\frac{1}{4}((\theta_y w+\theta_z v)(\theta_y\delta w+\theta_z\delta v)+(\theta_z u+\theta_x w)(\theta_z\delta u+\theta_x\delta w)))\mathrm{d}\Omega$;
- $\underline{\underline{M_{s,w}}} \propto \int_\Omega \tilde{\rho} w\delta w \mathrm{d}\Omega$;
- $\underline{\underline{N_{s,w}}} \propto \int_\Omega \tilde{\gamma}\frac{\partial p}{\partial z}\delta w \mathrm{d}\Omega$;

- $\underline{\underline{O_{s,w}}} \propto \int_\Omega \tilde{\gamma}\theta_3 p\delta w \mathrm{d}\Omega$;
- $\underline{\underline{T_{s,w}}} \propto \int_\Omega \phi(1+\frac{Q}{R})(\frac{\partial p}{\partial z}\delta w + p\frac{\partial \delta w}{\partial z})\mathrm{d}\Omega$;
- $\underline{\underline{K_f}} \propto \int_\Omega \frac{\phi^2}{\tilde{\rho_{22}}}(\frac{\partial p}{\partial x}\frac{\partial \delta p}{\partial x} + \frac{\partial p}{\partial y}\frac{\partial \delta p}{\partial y} + \frac{\partial p}{\partial z}\frac{\partial \delta p}{\partial z})\mathrm{d}\Omega$;
- $\underline{\underline{L_f}} \propto \int_\Omega \frac{\phi^2}{\tilde{\rho_{22}}} p(\frac{\partial \delta p}{\partial x}\theta_1 + \frac{\partial \delta p}{\partial y}\theta_2 + \frac{\partial \delta p}{\partial z}\theta_3) - (\frac{\partial p}{\partial x}\theta_1 + \frac{\partial p}{\partial y}\theta_2 + \frac{\partial p}{\partial z}\theta_3)\delta p \mathrm{d}\Omega$;
- $\underline{\underline{H_f}} \propto \int_\Omega \frac{\phi^2}{\tilde{\rho_{22}}} p\delta p \mathrm{d}\Omega$;
- $\underline{\underline{M_f}} \propto \int_\Omega \frac{\phi^2}{R} p\delta p \mathrm{d}\Omega$;
- $\underline{\underline{N_f}} \propto \int_\Omega \tilde{\gamma}(u\frac{\partial \delta p}{\partial x} + v\frac{\partial \delta p}{\partial y} + w\frac{\partial \delta p}{\partial z})\mathrm{d}\Omega$;
- $\underline{\underline{O_f}} \propto \int_\Omega \tilde{\gamma}(\theta_1 u + \theta_2 v + \theta_3 w)\delta p \mathrm{d}\Omega$;
- $\underline{\underline{T_f}} \propto \int_\Omega \phi(1+\frac{Q}{R})((\frac{\partial \delta p}{\partial x}u + \frac{\partial \delta p}{\partial y}v + \frac{\partial \delta p}{\partial z}w) + \delta p(\frac{\partial u}{\partial x} + \frac{\partial v}{\partial y} + \frac{\partial w}{\partial z}))\mathrm{d}\Omega$.

Acknowledgments

This project has received funding from the European Union's Horizon 2020 research and innovation program under the Marie Skłodowska-Curie grant agreement No. 675441.

References

[1] L. Cao, Q. Fu, Y. Si, B. Ding, J. Yu, Porous materials for sound absorption, Compos. Commun. 10 (2018) 25–35.

[2] X. D. Zhao, Y. J. Yu, Y. J. Wu, Improving low-frequency sound absorption of micro-perforated panel absorbers by using mechanical impedance plate combined with helmholtz resonators, Appl. Acoust. 114 (2016) 92–98.

[3] C. Cai, C. M. Mak, Noise attenuation capacity of a helmholtz resonator, Adv. Eng. Softw. 116 (2018) 60–66.

[4] F. Yildiz, A. G. Parlar, Z. Parlar, M. Bakkal, Properties of sound panels made from recycled footwear treads, Acta Phys. Pol. A 132 (3) (2017) 936–940.

[5] L. Lv, J. Bi, C. Wei, X. Wang, Y. Cui, H. Liu, Effect of micro-slit plate structure on the sound absorption properties of discarded corn cob husk fiber, Fibers Polym. 16 (7) (2015) 1562–1567.

[6] U. Berardi, G. Iannace, Acoustic characterization of natural fibers for sound absorption applications, Build. Environ. 94 (2015) 840–852.

[7] X. Xinzhao, L. Guoming, L. Dongyan, S. Guoxin, Y. Rui, Electrically conductive graphene-coated polyurethane foam and its epoxy composites, Compos. Commun. 7 (2018) 1–6.

[8] J.-P. Groby, B. N. C. Lagarrigue, B. Brouard, O. Dazel, et al., Using simple shape three-dimensional inclusions to enhance porous layer absorption, J. Acoust. Soc. Am. 136 (1139) (2014).

[9] Y. Yang, B. R. Mace, M. J. Kingan, Wave and finite element method for predicting sound transmission through finite multi-layered structures with fluid layers, Comput. Struct. (2018).

[10] T. Weisser, Acoustic behavior of a rigidly backed poroelastic layer with periodic resonant inclusions by a multiple scattering approach, J. Acoust. Soc. Am 139 (2) (2016) 617–629.

[11] M. Gaborit, O. Dazel, P. Göransson, A simplified model for thin acoustic screens, J. Acoust. Soc. Am. 144 (1) (1962) 76–81.

[12] J.-P. Groby, A. Wirgin, L. D. Ryck, W. Lauriks, R. P. Gilbert, Y. S. Xu, Acoustic response of a rigid-frame porous medium plate with a periodic set of inclusions, J. Acoust. Soc. Am. 126 (2) (2009) 685–693.

[13] L. Xiong, B. Nennig, Y. Aurégan, W. Bi, Sound attenuation optimization using metaporous materials tuned on exceptional points, J. Acoust. Soc. Am. 142 (4) (2017) 2288–2297.

[14] M. Biot, Mechanics of deformation and acoustic propagation in porous media, J. Appl. Physiscs 33 (4) (1962) 1482–1498.

[15] E. Detournay, A. H.-D. Cheng, Fundamentals of poroelasticity, Comprehensive Rock Engineering: Principles, Practice and Projects 2 (1993) 113–171.

[16] M. Collet, M. Ouisse, M. Ruzzene, M. N. Ichchou, Floquet-bloch decomposition for the computation of dispersion of two-dimensional periodic, damped mechanical systems, Int. J. Solids Struct. 48 (20) (2011) 2837–2848.

[17] K. Billon, M. Ouisse, E. Sadoulet-Reboul, M. Collet, P. Butaud, G. Chevallier, A. Khelif, Design and experimental validation of a temperature-driven adaptive phononic crystal slab, Smart Mat. and Struct. (in review) (2019) 1–23.

[18] M. Collet, M. Ouisse, F. Tateo, Adaptive metacomposites for vibroacoustic control applications, IEEE Sensors Journal 14 (7) (2014) 2145–2152.

[19] D. Magliacano, M. Ouisse, A. Khelif, S. D. Rosa, F. Franco, N. Atalla, M. Collet, Computation of dispersion diagrams for periodic porous materials modeled as equivalent fluids, Mech. Syst. Signal Process. 130 (2019) 692–706.

[20] E. Deckers, S. Jonckheere, D. Vandepitte, Modelling techniques for vibro-acoustic dynamics of poroelastic materials, Arch Comput. Methods Eng. 22 (2015) 183–236.

[21] J. F. Allard, N. Atalla, Propagation of sound in porous media: Modelling sound absorbing materials, 2^{nd} Edition, Wiley, 2009.

[22] N. Atalla, R. Panneton, P. Debergue, A mixed displacement-pressure formulation for poroelastic materials, J. Acoust. Soc. Am. 103 (3) (2002) 1444–1452.

[23] O. C. Zienkiewicz, T. Shiomi, Dynamic behaviour of saturated porous media; the generalized biot formulation and its numerical solution, International Journal of Rock Mechanics and Mining Sciences 21 (3) (1984).

[24] N. Atalla, M. A. Hamdi, R. Panneton, Enhanced weak integral formulation for the mixed (u,p) poroelastic equations, J. Acoust. Soc. Am. 109 (6) (2002) 3065–3068.

[25] Q. Serra, M. N. Ichchou, J. Deu, Wave properties in poroelastic media using a wave finite element method, J. Sound Vib. 335 (2015) 125–146.

[26] K. Billon, Composites périodiques fonctionnels pour l'absorption vibroacoustique large bande (2017).

[27] G. Floquet, Sur les équations différentielles linéaires à coefficients périodiques [On the linear differential equations with periodic coefficients], ann. sci. l'École norm. Supérieure 12 (2) (1881).

[28] A. Bensoussan, J. L. Lions, G. Papanicolaou, Asymptotic Analysis of Periodic Structures, Elsevier, 1978.

[29] F. Bloch, Uber die quantenmechanik der elektronen in kristallgittern [On the quantum mechanics of the electrons in crystal lattices], Z. Phys. 52 (1928) 555–600.

[30] D. L. Johnson, J. Koplik, R. Dashen, Theory of dynamic permeability and tortuosity in fluid-saturated porous media, J. Fluid Mech. 176 (1) (1987) 379–402.

[31] Y. Champoux, J. F. Allard, Dynamic tortuosity and bulk modulus in air-saturated porous media, J. Appl. Phys. 70 (4) (1991) 1975–1979.

[32] M. R. Stinson, The propagation of plane sound waves in narrow and wide circular tubes, and generalization to uniform tubes of arbitrary cross-sectional shape, J. Acoust. Soc. Am. 89 (2) (1991) 550–558.

[33] W. X. Zhong, F. W. Williams, On the direct solution of wave propagation for repetitive structures, J. Sound Vib. 181 (3) (1995) 485–501.

[34] N. Dauchez, S. Sahraoui, N. Atalla, Convergence of poroelastic finite elements based on biot displacement formulation, J. Acoust. Soc. Am. 109 (2001) 33–40.

List of Tables

1 Properties of a PU 60 foam. 11
2 Properties of the foam used in the validation with the work by Serra *et al.* [25]. 13
3 Properties of the air used in the validation with the work by Serra *et al.* [25]. 13

List of Figures

1 3D unit cell constituted by a 2 cm cube, homogeneous (on the left) and with a 5 mm radius cylindrical hole (on the right). . 11

2 Dispersion curves validation with JCA plots; here, the Biot curves are computed for a homogeneous PU 60 foam, with $E = 10^{15}$ Pa and structural loss factor = 0. 12

3 Dispersion curves validation with JCA plots; here, the Biot curves are computed for a PU 60 foam with a perfectly rigid cylindrical inclusion, with $E = 10^{15}$ Pa and structural loss factor = 0. 12

4 Dispersion curve comparison with the reference (WFEM by Serra *et al.* [25]), and analytical model; real part of the wavenumber. 14

5 Dispersion curve comparison with the reference (WFEM by Serra *et al.* [25]), and analytical model; imaginary part of the wavenumber. 14